

Assessment and Uncertainty Analysis of ROSA/LSTF Test on Pressurized Water Reactor 1.9% Vessel Upper Head Small-Break Loss-of-Coolant Accident

Takeshi Takeda

Abstract—An experiment utilizing the ROSA/LSTF (rig of safety assessment/large-scale test facility) simulated a 1.9% vessel upper head small-break loss-of-coolant accident with an accident management (AM) measure under the total failure of high-pressure injection system of emergency core cooling system in a pressurized water reactor. Steam generator (SG) secondary-side depressurization on the AM measure was started by fully opening relief valves in both SGs when the maximum core exit temperature rose to 623 K. A large increase took place in the cladding surface temperature of simulated fuel rods on account of a late and slow response of core exit thermocouples during core boil-off. The author analyzed the LSTF test by reference to the matrix of an integral effect test for the validation of a thermal-hydraulic system code. Problems remained in predicting the primary coolant distribution and the core exit temperature with the RELAP5/MOD3.3 code. The uncertainty analysis results of the RELAP5 code confirmed that the sample size with respect to the order statistics influences the value of peak cladding temperature with a 95% probability at a 95% confidence level, and the Spearman's rank correlation coefficient.

Keywords—LSTF, LOCA, uncertainty analysis, RELAP5.

I. INTRODUCTION

BEST estimate plus uncertainty method has gained growing interest in the licensing process for nuclear power plants [1]. In the field of nuclear thermal-hydraulics, experiments with a variety of test facilities are divided into such categories as an integral effect test [2], a separate effect test [3], and a combined effect test [4]. The integral effect test simulates the whole system of a nuclear reactor. By contrast, the separate effect test and the combined effect test usually represent one and several of the nuclear reactor components, respectively. Database obtained from the integral effect test should be employed for input uncertainty validation of physical models in thermal-hydraulic system codes. Besides, input uncertainty quantification of the system code physical models should be carried out using the data of the separate effect test and the combined effect test. After determining the judging criteria, it is necessary to verify that a specific experiment is suitable for the input uncertainty validation or quantification.

When considering the effect of scaling, the remaining issues are to appropriately extrapolate thermal-hydraulic phenomena observed in a scaled-down integral test facility to the conditions of the reference nuclear reactor on account of unavoidable

distortion in the design and construction of the integral test facility [5]. The ROSA/LSTF in Japan [6] simulates a typical 3,423 MW (thermal) Westinghouse-type four-loop pressurized water reactor (PWR) by a two-loop system model with full height and 1/48 in volume. The LSTF is larger than other major integral test facilities, such as PKL (primärkreisläufe versuchsanlage) with a volumetric scaling ratio of 1/145 in Germany [7] and ATLAS (advanced thermal-hydraulic test loop for accident simulation) with a volume scale factor of 1/288 in South Korea [8]. The LSTF, therefore, has the merit of well-simulating the thermal-hydraulic phenomena that may appear during accidents or transients of PWR.

This study focused on the assessment and uncertainty analysis of an integral effect test with the LSTF, taking into account incidents relevant to safety issues such as vessel head wall thinning at the Davis Besse reactor in the US in 2002 [9], [10]. Circumferential cracking of penetrating nozzle for control rod drive mechanism may cause a small-break loss-of-coolant accident (SBLOCA) with a break at the vessel upper head. The new regulatory requirements for the Japanese light-water nuclear power reactors [11] include the evaluation of the effectiveness of measures taken to avoid the core damage in the event of loss of the emergency core cooling system (ECCS) water injection function during small and medium break LOCAs. An experiment denoted as SB-PV-09 simulated a PWR 1.9% vessel upper head SBLOCA with an AM operator action in 2005. The break size is equivalent to the size of ejection of one entire penetration nozzle for control rod drive mechanism. Core exit thermocouples are utilized worldwide as a key indicator to initiate an AM operator action by detecting core temperature excursion during accidents or transients of PWR. SG secondary-side depressurization by means of steam discharge through the full opening of the relief valves in both SGs was initiated as the AM measure when the maximum core exit temperature reached 623 K; a criterion for Japanese PWR. Break size for the SB-PV-09 test was larger than that for other two LSTF tests on the vessel upper head SBLOCA; 0.5% for the test designated as SB-PV-02 in 1987 [12] and 1% for the test denoted as SB-PV-07 in 2005 [13]. While no AM action was taken in the SB-PV-02 test, coolant was manually injected from high-pressure injection system of ECCS into both cold legs as the AM measure at the maximum core exit temperature of 623 K in the SB-PV-07 test. Total failure of the high-pressure injection system of ECCS was included in the common condition of the three LSTF tests.

In this study, first, the author evaluated the SB-PV-09 test by

Takeshi Takeda is with Nuclear Regulation Authority, Roppongi, Minato-ku, Tokyo 106-8450, Japan (phone: 81-3-5114-2100; fax: 81-3-5114-2179; e-mail: takeda.takeshi4695@gmail.com).

reference to the matrix of the integral effect test as a guide for validating the thermal-hydraulic system code [2]. Second, the author conducted posttest analysis of the SB-PV-09 test by employing the RELAP5/MOD3.3 code [14] to assess the code predictive capability. Third, the author was just trying to create the phenomena identification and ranking table (PIRT) for individual components from the aspect of the significance of phenomena in identifying peak cladding temperature (PCT) as a safety-related parameter. Fourth, the author performed sensitivity and uncertainty analyses of the SB-PV-09 test with the RELAP5 code to investigate the influences of uncertain parameters, selected from the PIRT, on the PCT. Owing to the accident scenario differences, some of the uncertain parameters and ranges differed from those used in the author's previous work [15], [16] on the uncertainty analyses of the LSTF tests concerning the SBLOCAs with or without scram. The author examined further how the number of samples in relation to the order statistics influences the PCT. This paper is concerned with major consequences of the LSTF test and the calculations with the RELAP5 code.

II. ASSESSMENT OF INTEGRAL EFFECT TEST WITH LSTF

A. Outline of LSTF System

The reference PWR of the LSTF is Tsuruga Unit-2. As illustrated schematically in Fig. 1, the LSTF comprises of a pressure vessel, pressurizer (PZR), and primary loops. An active SG with 141 full-size U-tubes (inner-diameter of 19.6 mm each), primary coolant pump, and hot and cold legs, are included in each loop. A control rod guide tube (CRGT) forms the flow path between the upper head and the upper plenum. Eight CRGTs in the LSTF are attached to an upper core plate to simulate the CRGT in the reference PWR, as shown in Fig. 2. The LSTF has two bypass flow paths. One is the flow path between the upper head and the downcomer giving a bypass flow of 0.3% of the total core flow rate during initial steady-state. The other is the flow path between the hot leg leak line and the downcomer allowing a 0.2% bypass flow for each loop. The horizontal cross-section of the LSTF core is presented in Fig. 3. The rod bundles designated as B13–B20, B21–B24, and B01–B12, are used for high-, mean-, and low-power rod bundles, respectively. The axial profile of the LSTF core power is organized in a nine-step chopped cosine in which a peaking factor is 1.495. The LSTF is equipped with all types of ECCS furnished to the reference PWR.

The following are the atypical features of the LSTF. The LSTF initial core power is 10 MW that is 14% of the volumetric-scaled (1/48) nominal core power of the reference PWR. Volume distribution in the pressure vessel of the LSTF differs from that of the reference PWR. The aspect ratio of the upper plenum in the LSTF, for example, is smaller than that in the reference PWR. Metal stored heat per unit volume of the primary coolant in the LSTF is greater than that in the reference PWR. Initial SG secondary-side pressure of the LSTF is 7.3 MPa due to the limitation of the primary-to-secondary heat transfer rate of 10 MW, whereas the nominal value is 6.1 MPa

for the reference PWR.

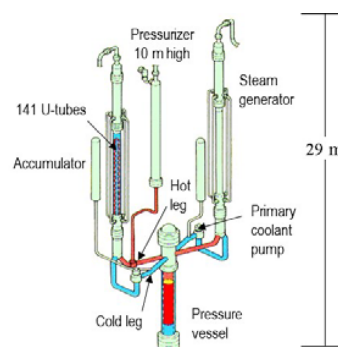


Fig. 1 Schematic view of ROSA/LSTF

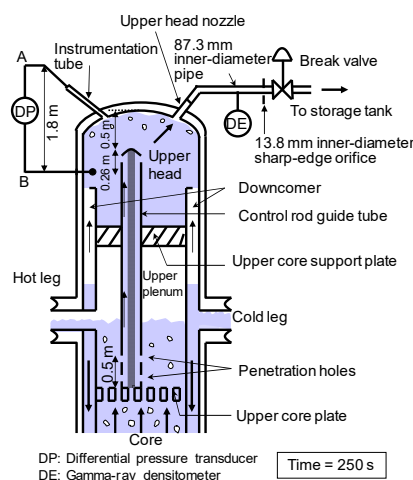


Fig. 2 Schematic view of LSTF pressure vessel and break unit

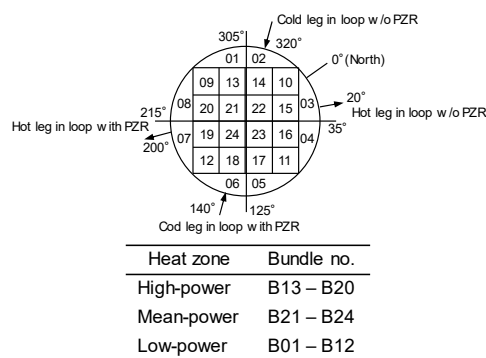


Fig. 3 Horizontal cross-section of LSTF test

B. Description of LSTF Test against Major Criteria for Selection of Appropriate Experiment

The major criteria for selecting an appropriate integral effect test involved geometry, scale, instrumentation, available measurements, range of main parameters, validation of complete system, covered phenomena and models, and available documentation and publications, referring to the matrix of the integral effect test for the thermal-hydraulic

system code validation [2]. The following is the description of the LSTF experiment against the major criteria.

1) Geometry

Four primary loops of Westinghouse-type PWR are represented by two equal-volume loops to simulate two-phase flows during accidents or transients. The full assembly has mostly the same dimensions as those of the Westinghouse-type PWR 17 × 17 fuel assembly to preserve the heat transfer characteristics of the core. The core, 3.66 m in active height, consists of 1,008 electrically-heated rods in 24 rod bundles to simulate the fuel rod assembly in the Westinghouse-type PWR.

2) Scale

The LSTF is designed to model the full-height primary system of the Westinghouse-type PWR. The volumetric scaling ratio of the primary loops is 1/48 of the Westinghouse-type PWR. Flow area in the horizontal leg is scaled to conserve the ratio of the length to the square-root of the pipe diameter of the Westinghouse-type PWR to better simulate the flow regime transitions in the primary loops (Froude number basis) [17]. The time scale of simulated phenomena is one to one to those in the Westinghouse-type PWR.

3) Instrumentation

There are a large number of instruments installed in the LSTF, such as pressure transducer, differential pressure transducer, thermocouple, flow meter, gamma-ray densitometer, electric power meter, magnetic pickup, and level meter. The gamma-ray densitometer uses certain conversion equations, considering attenuation effects of gamma-ray that goes through coolant flow. Visual observation of flow in the horizontal legs has only been possible by means of a periscope that withstands high-temperature steam/water conditions.

4) Available Measurements

The available measurements involve pressure, differential pressure, fluid temperature, wall temperature, flow rate, liquid level, fluid density, electric power, and pump rotation speed. Some parameters (e.g. liquid level that employs differential pressure cell data) require the calculation of the single-phase coolant density built on local pressure and fluid temperature data using steam table. The measurement uncertainty is estimated based on the accuracy of the related instrument [6]. As shown in Table I, sufficient measurement precision of the typical parameter was ensured, thereby proving the consistency of the measured data.

5) Range of Main Parameters

Some examples of the range of the main parameters defined in the SB-PV-09 test are outlined below. Throughout the experiment the core power is equal to or less than 10 MW. Until 1,800 s including core uncover and core reflooding periods after the test initiation, the range was 1.8–15.5 MPa for the primary pressure, 2.2–8.1 MPa for the SG secondary-side pressure, 480–748 K for the core exit temperature, and 480–975 K for the cladding surface temperature of simulated fuel rods. Such experimental data over a wide range should be helpful in

understanding several phenomena.

TABLE I
MEASUREMENT UNCERTAINTY OF TYPICAL PARAMETER

Parameter	Uncertainty	Parameter	Uncertainty
Core power	±0.07 MW	Primary loop mass flow rate	±1.25 kg/s
Horizontal leg fluid temperature	±2.75 K	Flow rate through SG relief valve	±0.07 kg/s
Core exit temperature	±3.49 K	Upper plenum collapsed liquid level	±0.197 m
Cladding surface temperature	±5.31 K	Core collapsed liquid level	±0.216 m
Primary pressure	±0.108 MPa	Hot leg liquid level	±0.012 m
Injection pressure of ACC system	±0.054 MPa	Cold leg liquid level	±0.028 m
SG secondary-side pressure	±0.054 MPa	Crossover leg downflow-side collapsed liquid level	±0.207 m

6) Validation of Complete System

After the test data acquisition, some experimental data are calibrated. The high-range pressure data in the PZR and the upper plenum, for example, are corrected on the basis of a zero level shift employing the low-range pressure data first, and then all the fluid density data are calibrated at two points under different fluid conditions. The experimental data are manually qualified through the comparison of the published ranges and uncertainty values [6]. Finally, available experimental data are obtained by excluding bad trend data from all the test data.

7) Covered Phenomena and Models

The covered phenomena and models specific to the SB-PV-09 test will be mentioned in Section V A. The covered phenomena resulting from the PIRT are to be shown in Table III. High-, medium-, and low-ranked phenomena respectively, may have large, medium, and small influences on the PCT. The covered models in the RELAP5 code to predict the covered phenomena included a two-phase critical flow model, gas-liquid inter-phase drag model and film boiling and steam convective heat transfer model.

TABLE II
CHRONOLOGY OF MAJOR EVENTS IN LSTF TEST AND POSTTEST ANALYSIS WITH RELAP5 CODE

Event	Experiment (s)	Calculation (s)
Break valve open	0	0
Generation of scram signal	22	20
Break flow from single-phase liquid to two-phase flow	50	45
Start of significant drop in upper plenum liquid level	650	525
Break flow from two-phase flow to single-phase vapor	700	665
Upper plenum became empty of liquid.	780	700
Start of increase in cladding surface temperature	840	905
Start of increase in core exit temperature	900	920
Start of SG secondary-side depressurization	1,090	1,155
PCT appeared	1,220	1,350
Actuation of ACC system	1,300	1,490
Loop seal clearing	1,400	1,500
Whole core was quenched.	1,550	1,520

TABLE III
PIRT AND RELATED UNCERTAIN PARAMETERS

Component	Phenomenon	Rank*	Parameter
Break	Critical flow	H	Break discharge coefficient for single-phase liquid and two-phase flow
Upper head	Two-phase mixture level	M	Gas-liquid inter-phase drag in upper head
	Horizontal stratification	L	Gas-liquid relative velocity in upper head
Upper plenum	Two-phase mixture level	M	Gas-liquid inter-phase drag in upper plenum
	Horizontal stratification	L	Gas-liquid relative velocity in cold leg
Fuel rods	Decay heat	H	Core decay power
	Stored heat	M	Thermal conductivity of fuel rod
			Heat capacity of fuel rod
Core	Two-phase mixture level	H	Gas-liquid inter-phase drag in core
	Heat transfer	H	Film boiling and steam convective heat transfer coefficients in core
	Rewet	M	Boiling heat flux in core
Downcomer	Two-phase mixture level	M	Gas-liquid inter-phase drag in downcomer
	Bypass flow between upper head and downcomer	M	Form loss coefficient in upper head spray nozzle
	Bypass flow between hot leg leak line and downcomer	L	Form loss coefficient in hot leg nozzle
Pressurizer	Two-phase mixture level	L	Gas-liquid inter-phase drag in pressurizer
Hot leg	Horizontal stratification	L	Gas-liquid relative velocity in hot leg
SG	Steam discharge through SG secondary-side valve	H	Discharge coefficient through SG relief valve during SG secondary-side depressurization
	Steam condensation in SG U-tubes	H	Core exit temperature that initiated SG secondary-side depressurization
Crossover leg	Horizontal stratification	L	Gas-liquid relative velocity in crossover leg
Cold leg	Steam condensation on ACC coolant	M	Injection pressure of ACC system
	Horizontal stratification	L	Gas-liquid relative velocity in cold leg
Primary coolant pump	Flow resistance	L	Resistance coefficient in primary coolant pump
	Coastdown performance	L	Rotation speed of primary coolant pump

* H, high-ranked phenomenon; L, low-ranked phenomenon; M, medium-ranked phenomenon

8) Available Documentation and Publications

The NEA/CSNI (nuclear energy agency/committee on the safety of nuclear installation) documentation [18] giving an account of the SB-PV-09 test, was available worldwide for better understanding of the phenomena involved, because the SB-PV-09 test was carried out for the OECD/NEA ROSA Project. The relevant publications [19]-[21] contained some information derived from the posttest calculations with different thermal-hydraulic system codes of TRACE and ATHLET against the SB-PV-09 test.

In summary, the SB-PV-09 test met the requirements for the proper integral effect test through the description of the experiment against the major criteria 1) –8) mentioned above. The LSTF experimental database on the vessel upper head SBLOCA with the AM action will be useful for studying reliable safety assurance measures in PWR accidents with severe multiple system failures.

III. LSTF TEST AND RELAP5 CODE ANALYSIS CONDITIONS

A. LSTF Test Conditions

A 13.8 mm inner-diameter, sharp-edge orifice was mounted on the downstream of a horizontal pipe that was connected to an upper head nozzle through an oblique pipe, as shown in Fig. 2. The orifice size was equivalent to 1.9% of the volumetrically-scaled cross-sectional area of the reference PWR cold leg. At time zero, initial PZR pressure of 15.5 MPa agreed with the reference PWR condition. The SG secondary-side pressure of 8.03 MPa and 7.82 MPa corresponded to setpoint pressure for opening and closure of SG relief valves respectively, while

referring to the setpoint value used in the reference PWR. Loss of off-site power was supposed to occur simultaneously with a scram signal when the PZR pressure decreased to 12.97 MPa. The LSTF core power decay curve after the scram signal was predetermined founded on some calculations with the RELAP5 code [22]. Relief valves in both SGs were fully opened as the AM measure at the maximum core exit temperature of 623 K, while injecting auxiliary feedwater into the secondary-side of both SGs. Accumulator (ACC) system of ECCS automatically initiated coolant injection at a constant temperature of 320 K into both cold legs when the primary pressure decreases to 4.51 MPa.

B. RELAP5 Calculation Conditions

The RELAP5/MOD3.3 code with a two-phase critical flow model was employed for the calculations of the LSTF test. The Bernoulli incompressible orifice flow equation is used for single-phase discharge liquid [23]. An attempt was made to apply the maximum bounding flow theory to two-phase discharge flow [24]. The values of the discharge coefficient (C_d) employed for single-phase discharge liquid, two-phase discharge flow, and single-phase discharge steam were 0.61, 0.61, and 0.84 [25], respectively.

A nodding schematic of the LSTF system for the RELAP5 code analysis is shown in Fig. 4. The characteristics of the considered pressure vessel nodalization are presented in the following. It was faithfully modeled that the break located at the end of the horizontal pipe was connected to the upper head through the oblique pipe. The upper head placed above the CRGT was divided into ten equal-height volumes to better

simulate the upper head collapsed liquid level. Flow paths between the upper plenum and the CRGT were modeled to reproduce the coolant flow at the penetration holes placed at the CRGT bottom. The core was split into nine equal-height volumes that were vertically stacked according to a nine-step chopped cosine power profile along the core length. When the maximum cladding surface temperature was above 958 K, no automatic decrease in the core power was assumed to avoid the power reduction effect in the calculation only. Other initial and boundary conditions agreed to the LSTF test conditions.

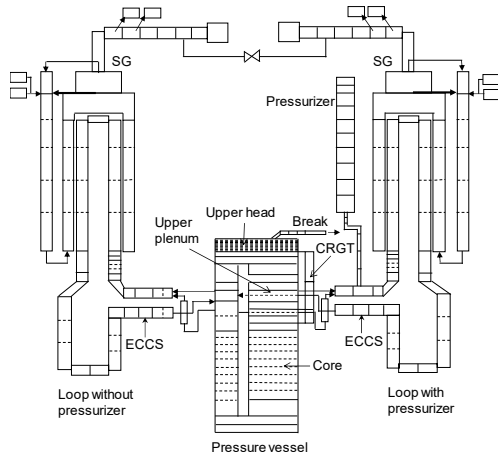


Fig. 4 Noding schematic of LSTF system for RELAP5 code analysis

IV. LSTF TEST AND RELAP5 CODE ANALYSIS RESULTS

A. Major Phenomena Specific to LSTF Test

Figs. 5-12 show the major phenomena specific to the LSTF test. The primary pressure began to decrease after the break, whereas the SG secondary-side pressure raised up to 8 MPa soon after the closure of the SG main steam isolation valves in the scram signal (Fig. 5). Until 1,090 s when the AM action was instituted, the SG secondary-side pressure fluctuated between 8.03 MPa and 7.82 MPa by cycle opening of the SG relief valve, which resulted in the primary pressure fluctuation. The break flow rate roughly decreased stepwise when the break flow turned from single-phase liquid to two-phase flow at 50 s, and then changed to single-phase vapor at 700 s (Fig. 6). The primary pressure became lower than the SG secondary-side pressure at around 800 s, that is, a little before the initiation of core uncover (Figs. 5, 8, and 10). This resulted in no reflux flow from the SG. Until around 1,200 s after the AM action onset, the AM action was ineffective on the intended primary depressurization to initiate the ACC coolant injection. The reason for this ineffectiveness was because the SG secondary-side pressure was higher than the primary pressure during that time period.

The liquid level in the upper head is evaluated from the measured differential pressure between symbols A and B shown in Fig. 2. The upper head liquid level affected the break flow rate as coolant in the upper plenum flowed into the upper head through the CRGTs until the penetration holes placed at the CRGT bottom were filled with steam in the upper plenum

(Fig. 6). Oscillation in the upper head mixture level gave rise to the oscillation in the break flow rate through the break-upstream fluid density (Fig. 7). The oscillation in the upper head mixture level was attributed to the primary pressure fluctuation because of the SG relief valve cycle opening. Fig. 2 contains the sketch of the primary coolant distribution estimated on the basis of measured data typically at 250 s. The upper plenum collapsed liquid level was maintained constant at the penetration holes located at the CRGT bottom for a short while around 670-720 s (Fig. 8).

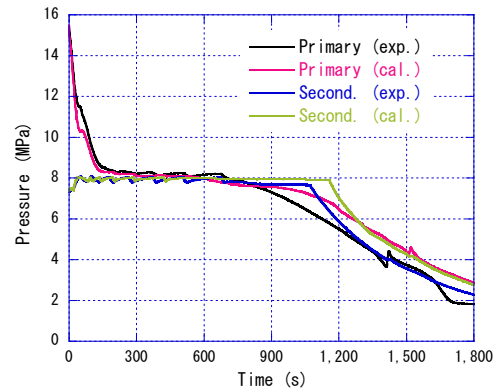


Fig. 5 Test and calculated results for primary and SG secondary-side pressures in loop with PZR

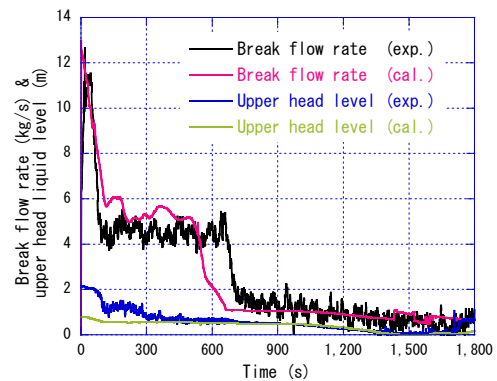


Fig. 6 Test and calculated results for break flow rate and upper head collapsed liquid level

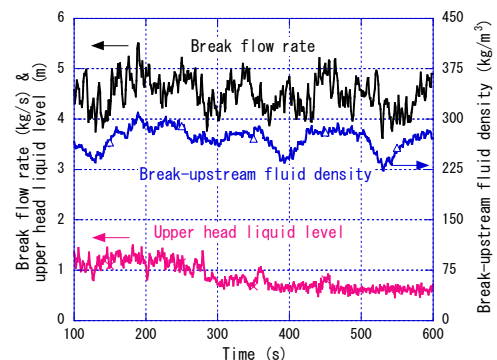


Fig. 7 Test results for break flow rate, break-upstream fluid density, and upper head collapsed liquid level

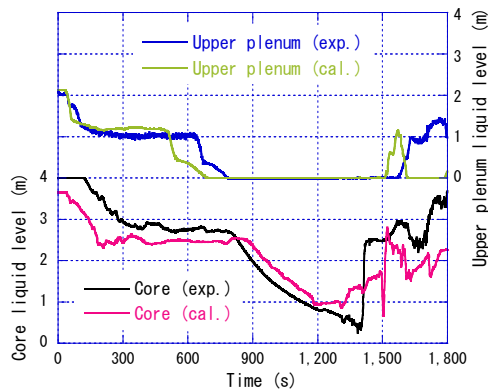


Fig. 8 Test and calculated results for collapsed liquid levels of upper plenum and core

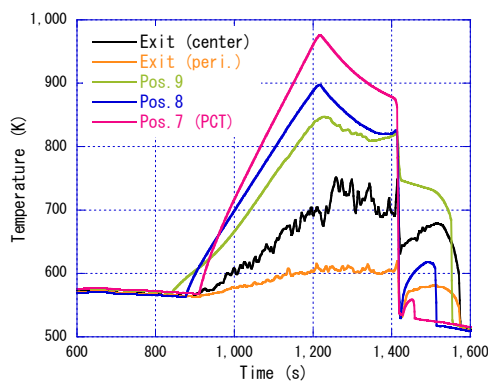


Fig. 9 Test results for core exit temperatures and cladding surface temperatures

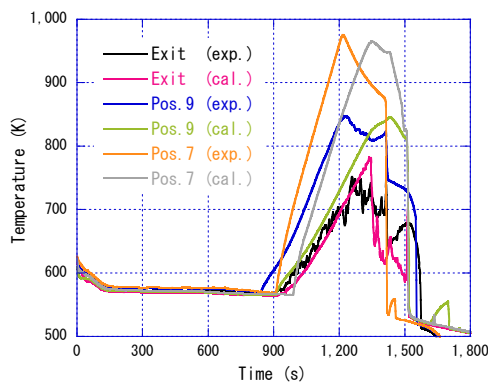


Fig. 10 Test and calculated results for core exit temperature and cladding surface temperatures

Core uncover occurred by core boil-off after the upper plenum became voided (Figs. 8-10). The core exit temperature started to increase at 900 s, at around the center of the upper core plate above the B21 rod bundle (Fig. 3) where the peak temperature was observed (Fig. 9). By contrast, the cladding surface temperature at Position 9 (= about 3.6 m above the core bottom) in the B17 rod bundle (Fig. 3), began to increase at 840 s. There was the time delay in detecting steam superheating by

utilizing the core exit thermocouples. The causes of the time delay included core power distribution, three-dimensional steam flow in the core because of steam flow towards the break through the CRGTs, low-temperature steam flow from the core peripheral region, and low-temperature metal structure around the core exit. The stepwise reduction in the core power was made to protect the LSTF core because the maximum cladding surface temperature exceeded the predetermined criterion of 958 K. The peak core exit temperature was 748 K at 1,275 s. The PCT, which was observed at Position 7 (= about 2.6 m above the core bottom) in the B17 rod bundle (Fig. 3), was 975 K at 1,220 s.

As shown in Fig. 11, the ACC system intermittently actuated in both loops during the time periods around 1,300-1,420 s and 1,500-1,800 s, in response to the primary pressure. The primary depressurization was enhanced because of significant condensation of steam on the ACC coolant injected into both cold legs. Loop seal clearing in both loops at 1,400 s was induced by the significant condensation of steam on the ACC coolant in both the cold legs (Fig. 12). The core liquid level recovered after the loop seal clearing in both loops. The core exit temperature was maintained at the saturation temperature after 1,575 s, whereas the whole core was quenched by 1,550 s. An early SG secondary-side depressurization by the full opening of the SG secondary-side valves [26] as an AM measure will be needed to avoid a significant increase in the cladding surface temperature in this type of vessel upper head SBLOCA with totally-failed high-pressure injection system.

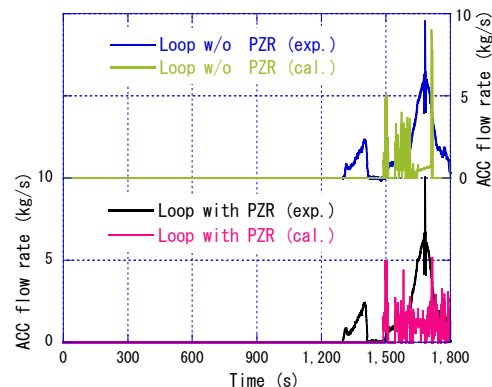


Fig. 11 Test and calculated results for injection flow rates of ACC system in both loops

B. Assessment of RELAP5 Code Predictive Capability

The SG secondary-side pressure was calculated reasonably well, resulting from good prediction of the cycle opening of the SG relief valve (Fig. 5). As shown in Table II, however, there were some discrepancies from the measured data in the timings of major events. The code also under-predicted the primary pressure due to the over-prediction of the break flow rate during two-phase flow discharge period (Figs. 5 and 6). The upper head collapsed liquid level was not well calculated during two-phase flow discharge period (Fig. 6). Consequently, the upper plenum collapsed liquid level began to significantly drop earlier

in the calculation compared to the LSTF test (Fig. 8). The code qualitatively reproduced that the upper plenum collapsed liquid level was maintained constant at the penetration holes placed at the CRGT bottom (Fig. 8).

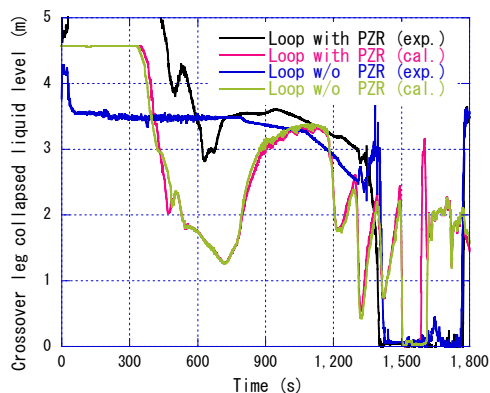


Fig. 12 Test and calculated results for crossover leg downflow-side collapsed liquid levels in both loops

The cladding surface temperature began to rise later in the calculation compared to the LSTF test due to the over-prediction of the core liquid level, which resulted in the over-prediction of the primary pressure (Figs. 5, 8, and 10). The code roughly predicted the time delay until the start of the core exit temperature rise after the initiation of the cladding surface temperature increase (Fig. 10). The difficulty of predicting multi-dimensional steam flow in the core, however, caused that the increase rate of the core exit temperature was larger in the calculation compared to the LSTF test (Fig. 10). The PCT appeared at the node of Position 7 (= about 2.4–2.8 m above the core bottom) in the calculation, and the PCT was observed at Position 7 in the LSTF test (Fig. 10). The PCT was under-predicted due to the insufficient predictions of the collapsed liquid levels of the crossover leg downflow-side and the core (Figs. 8, 10, and 12). Owing to the inadequate prediction of the

ACC injection flow rate, the whole core was quenched earlier in the calculation compared to the LSTF test, whereas the ACC system actuated later in the calculation (Figs. 10 and 11).

V. SENSITIVITY AND UNCERTAINTY ANALYSES WITH RELAP5 CODE

A. Sensitivity and Uncertainty Analysis Conditions

The author tried to make the PIRT for each component from the standpoint of the significance of phenomena to determine the PCT, taking account of the LSTF test data analysis and the RELAP5 posttest calculation. The range and distribution for each relevant uncertain parameter were considered based on the PIRT. As indicated in Table III, the high-ranked phenomena, which may affect largely the PCT, included critical flow at the break, decay heat of the fuel rods, core two-phase mixture level, core heat transfer, steam discharge through the SG secondary-side valve, and steam condensation in the SG U-tubes during the SG secondary-side depressurization.

Table IV shows the range and distribution for each uncertain parameter applied to the high-ranked phenomenon. The C_d through the break for single-phase liquid and two-phase flow was in the range of 0.57 to 0.65, on the basis of some trial calculations. The range of the core decay power was the specified value ± 0.07 MW in accordance with the measurement uncertainty [6]. The gas-liquid inter-phase drag in the core ranged from 70% to 130% because of the unknown uncertainty of the inter-phase drag model in the code. The film boiling and steam convective heat transfer coefficients in the core were in the range of 70% to 130% owing to the indefinite uncertainty of the heat transfer models in the code. The C_d through the SG relief valve during the SG secondary-side depressurization ranged from 0.8 to 0.88, through some trial calculations. The range of the core exit temperature that initiated the SG secondary-side depressurization was 623 ± 3 K, according to the measurement uncertainty [6].

TABLE IV
RANGE AND DISTRIBUTION FOR UNCERTAIN PARAMETER

Parameter	Base Case Value	Range	Distribution
Discharge coefficient through break for single-phase liquid and two-phase flow	0.61	[0.57, 0.65]	Uniform
Core decay power	Specified value MW	$[-0.07, +0.07]$ MW	Normal
Gas-liquid inter-phase drag in core	100%	[70, 130]%	Normal
Film boiling and steam convective heat transfer coefficients in core	100%	[70, 130]%	Normal
Discharge coefficient through SG relief valve during SG secondary-side depressurization	0.84	[0.8, 0.88]	Uniform
Core exit temperature that initiated SG secondary-side depressurization	623 K	[620, 626] K	Normal

The measurement uncertainty or the unknown uncertainty of the physical models in the code was associated with the ranges for the core decay power, the gas-liquid inter-phase drag in the core, the film boiling and steam convective heat transfer coefficients in the core, and the core exit temperature that initiated the SG secondary-side depressurization. For that reason, the normal distribution was implemented in the distribution for the four uncertain parameters. The C_d through the break for single-phase liquid and two-phase flow and the C_d

through the SG relief valve during the SG secondary-side depressurization respectively, had influences on the code predictability for critical flow and steam discharge through the SG relief valve. On this account, the uniform distribution was applied to the distribution for the two uncertain parameters.

The necessary number n of the computer code runs was determined through the application of the following formula for the p th order by Guba et al. [27].

$$\sum_{j=0}^{n-p} \frac{n!}{(n-j)!j!} \alpha^j (1-\alpha)^{n-j} \geq \beta, \quad (1)$$

where α is the probability and β is the confidence level. The required number of the computer code calculations with a probability of 95% at a confidence level of 95% was 59, 93, and 124 respectively for the first, second, and third order. For the 93-sample case, 34 new calculations were added to the 59 computer code runs. For the 124-sample case, 31 additional calculations were added to the 93 calculated runs. To propagate input uncertainties, a random value for each set of the uncertain parameters was produced by making use of the Latin hypercube sampling [28]; an effective multi-dimensional and hierarchical sampling method.

B. Influences of Uncertain Parameter on Cladding Surface Temperature

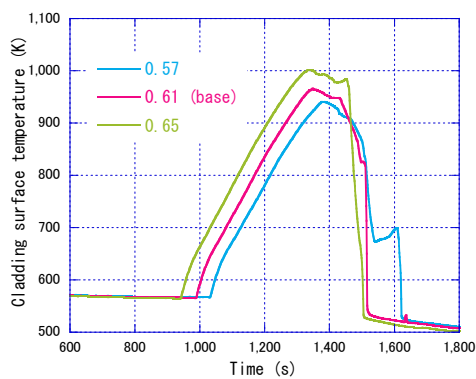


Fig. 13 Discharge coefficient through break versus cladding surface temperature by sensitivity analysis

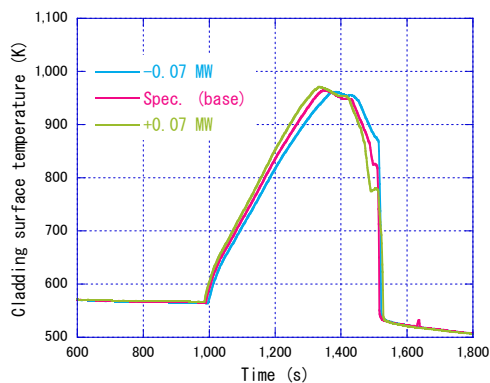


Fig. 14 Core decay power versus cladding surface temperature by sensitivity analysis

Figs. 13-18 compare the results of the sensitivity analysis and the posttest analysis as the base case calculation for the cladding surface temperature at the node of Position 7, where the PCT appeared, in terms of each uncertain parameter. As for the C_d through the break for single-phase liquid and two-phase flow, the cladding surface temperature started to increase later when the C_d was 0.57, while it began to rise earlier in the case of the C_d of 0.65, as compared to the base case of 0.61 (Fig. 13).

The PCT was lower for the C_d of 0.57, while it was higher for the C_d of 0.65, as opposed to the base case of 0.61. Regarding the core decay power, the cladding surface temperature started to increase later in the case of the specified value minus 0.07 MW, while it began to rise earlier in the case of the specified value plus 0.07 MW, as compared to the base case of the specified value (Fig. 14). Some differences appeared in the cladding surface temperature increase rates among the cases of the specified value minus 0.07 MW, the specified value, and the specified value plus 0.07 MW. There was no apparent relationship between the gas-liquid inter-phase drag in the core and the PCT in the cases of the 70%, 100%, and 130% inter-phase drags (Fig. 15). Concerning the film boiling and steam convective heat transfer coefficients in the core, the PCT was higher in the case of the 70% heat transfer coefficients, while it was lower in the case of the 130% heat transfer coefficients, as opposed to the base case of 100% (Fig. 16). With regard to the C_d through the SG relief valve during the SG secondary-side depressurization, the PCT was higher for the C_d of 0.8, while it was lower for the C_d of 0.88, as compared to the base case of 0.84 (Fig. 17). As for the core exit temperature that initiated the SG secondary-side depressurization, the PCT was lower in the case of the temperature of 620 K, while it was higher in the case of the temperature of 626 K, as opposed to the base case of 623 K (Fig. 18).

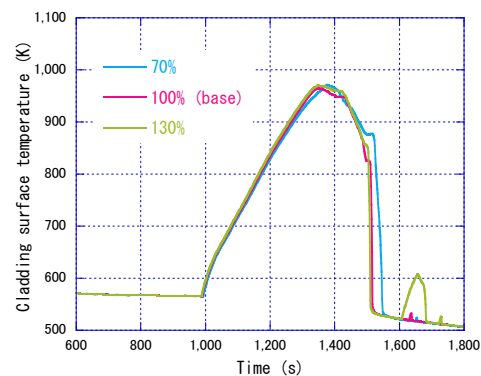


Fig. 15 Gas-liquid inter-phase drag in core versus cladding surface temperature by sensitivity analysis

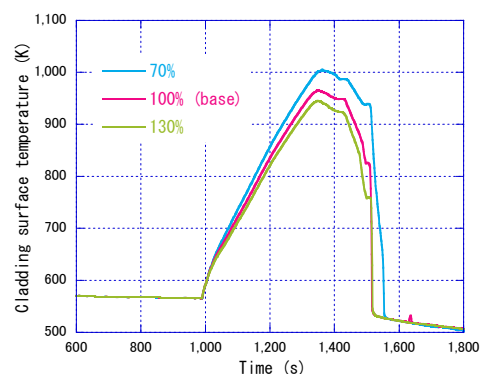


Fig. 16 Film boiling and steam convective heat transfer coefficients in core versus cladding surface temperature by sensitivity analysis

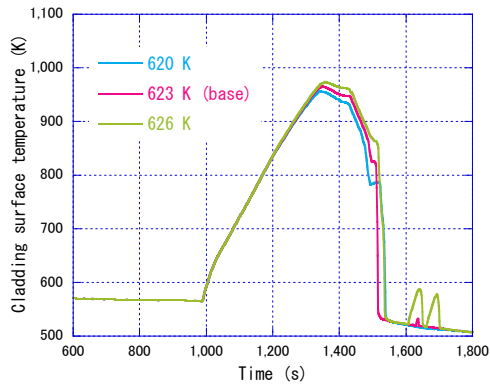


Fig. 17 Core exit temperature that initiated SG secondary-side depressurization versus cladding surface temperature by sensitivity analysis

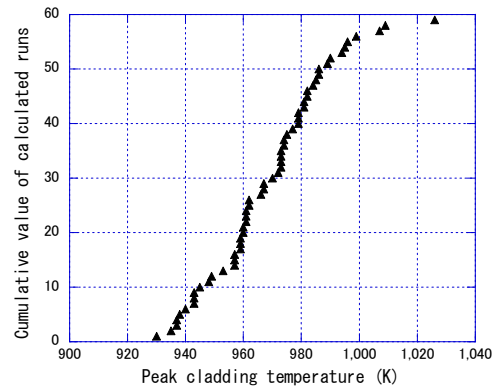


Fig. 19 Relationship between PCT and cumulative value of calculated runs in 59-sample case

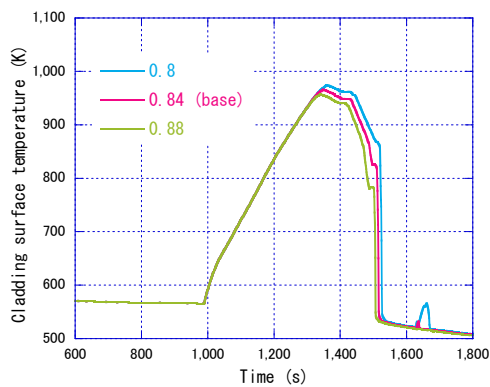


Fig. 18 Discharge coefficient through SG relief valve during SG secondary-side depressurization versus cladding surface temperature by sensitivity analysis

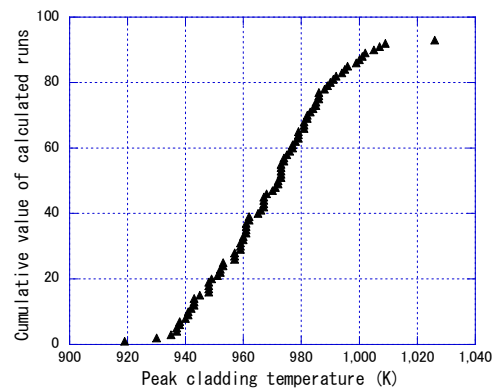


Fig. 20 Relationship between PCT and cumulative value of calculated runs in 93-sample case

C. Influences of Sample Size on PCT

Figs. 19-21 respectively indicate the relationship between the PCT and the cumulative value of 59, 93, and 124 samples. The distribution was random for frequency at certain values of the calculated PCT in either case. The experimental PCT of 975 K was a value between the calculated minimum and maximum PCTs in either case, as shown in Table V. The standard deviation of the PCT as well as the averaged PCT was much the same in the three cases of different sample sizes. This revealed no apparent relationship between the dispersion of the PCT and the sample size.

TABLE V
PCT IN THREE CASES OF DIFFERENT SAMPLE SIZES

Item	59-sample case	93-sample case	124-sample case
Averaged PCT	969 K	969 K	969 K
Standard deviation of PCT	20 K	21 K	21 K
Maximum PCT	1,026 K	1,026 K	1,026 K
Second-maximum PCT	1,009 K	1,009 K	1,021 K
Third-maximum PCT	1,007 K	1,007 K	1,017 K
Fourth-maximum PCT	999 K	1,005 K	1,009 K
Fifth-maximum PCT	996 K	1,002 K	1,007 K
Minimum PCT	930 K	919 K	919 K

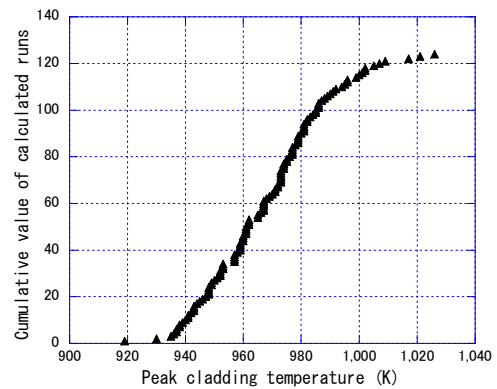


Fig. 21 Relationship between PCT and cumulative value of calculated runs in 124-sample case

Figs. 22-24 respectively present the results from the maximum to fifth-maximum PCTs in the cases of 59, 93, and 124 samples, being compared to the base case calculation. For the 59-, 93-, and 124-sample cases, the calculated maximum, second-maximum, and third-maximum PCTs respectively, were 1,026 K, 1,009 K, and 1,017 K. These PCTs corresponded to the values of PCT with a probability of 95% at a confidence level of 95% [29]. The PCT values with a 95% probability at a

95% confidence level should differ greatly due to the sample size difference, thereby influencing the margin to the acceptance criterion of the PCT. In the 59-sample case, the difference between the maximum and second-maximum PCTs was 17 K. In the 93-sample case, the difference between the second- and third-maximum PCTs was 2 K, while that between the maximum and second-maximum PCTs was 17 K. In the 124-sample case, the difference between the third- and fourth-maximum PCTs was 8 K, while that between the second- and third-maximum PCTs was 4 K. These suggest that the 124-sample case should be better than the 59- and 93-sample cases in terms of the representational to the PCT value with a 95% probability at a 95% confidence level.

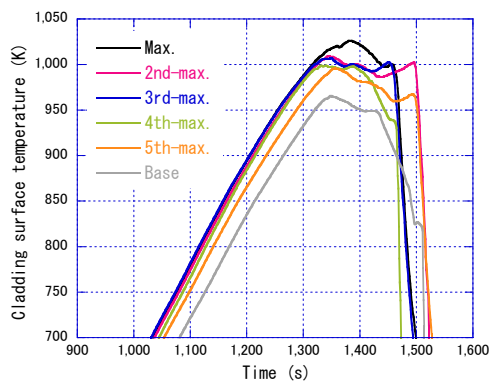


Fig. 22 Results from the maximum to fifth-maximum PCTs in 59-sample case

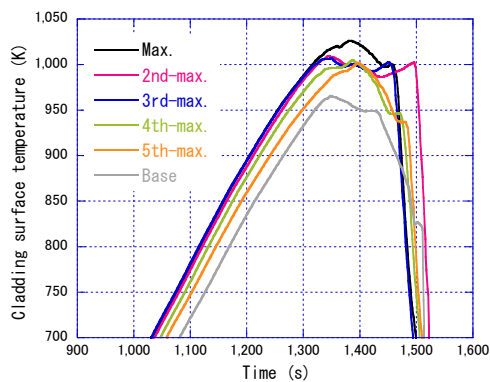


Fig. 23 Results from the maximum to fifth-maximum PCTs in 93-sample case

Table VI shows the uncertain parameters versus the PCTs in the 124-sample case. When the PCTs were from the maximum to fifth-maximum ones, the range was 0.635–0.650 for the C_d through the break for single-phase liquid and two-phase flow, was 76.1–92.6% for the film boiling and steam convective heat transfer coefficients in the core, and was 0.802–0.851 for the C_d through the SG relief valve during the SG secondary-side depressurization. This implies that the PCT should be considerably higher when the C_d through the break for single-phase liquid and two-phase flow is quite large, and the film boiling and steam convective heat transfer coefficients in

the core, and the C_d through the SG relief valve during the SG secondary-side depressurization are relatively smaller within the specified uncertain ranges.

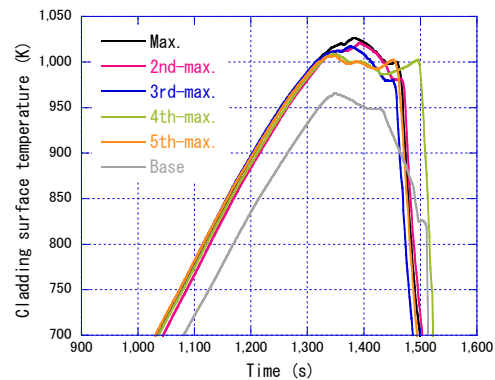


Fig. 24 Results from the maximum to fifth-maximum PCTs in 124-sample case

The author identified the strength of the relationship between the two sets of data for application of the following Spearman's rank correlation coefficient r_s [30].

$$r_s = 1 - \frac{6 \sum_i (x_i - y_i)^2}{n_s (n_s^2 - 1)}, \quad (2)$$

where x is the rank of the input variable (i.e. the uncertain parameter), y is the rank of the output variable (i.e. the PCT), and n_s is the number of data sets (i.e. the number of the calculated runs).

Table VII shows the r_s values for the C_d through the break for single-phase liquid and two-phase flow, the core decay power, the core inter-phase drag, the film boiling and steam convective heat transfer coefficients in the core, the C_d through the SG relief valve during the SG secondary-side depressurization, and the core exit temperature that initiated the SG secondary-side depressurization. These r_s values, respectively, were estimated to be 0.82, 0.17, -0.01, -0.48, -0.24, and 0.19 in the 59-sample case, to be 0.85, 0.19, 0.07, -0.45, -0.29, and 0.15 in the 93-sample case, and to be 0.79, 0.13, 0.03, -0.51, -0.27, and 0.13 in the 124-sample case. Some differences appeared in the r_s values for each uncertain parameter among the three cases of different sample sizes, but the tendencies of the r_s values were the same in the three cases. The correlation with the PCT is higher as the absolute value of r_s is larger. The highest, second-highest, and third-highest sensitive parameters to the PCT thus were the C_d through the break for single-phase liquid and two-phase flow, the film boiling and steam convective heat transfer coefficients in the core, and the C_d through the SG relief valve during the SG secondary-side depressurization, respectively. By contrast, the core decay power, the core inter-phase drag, and the core exit temperature that initiated the SG secondary-side depressurization had a low correlation with the PCT because the absolute value of r_s was below 0.2. Consequently, the author made clear that the PCT largely depended on the

combination of the C_d through the break for single-phase liquid and two-phase flow, the film boiling and steam convective heat transfer coefficients in the core, and the C_d through the SG

relief valve during the SG secondary-side depressurization within the limited uncertain ranges.

TABLE VI
UNCERTAIN PARAMETERS VERSUS PCT IN 124-SAMPLE CASE

Parameter	Maximum (1,026 K)	Second-maximum (1,021 K)	Third-maximum (1,017 K)	Fourth-maximum (1,009 K)	Fifth-maximum (1,007 K)
Discharge coefficient through break for single-phase liquid and two-phase flow	0.645	0.635	0.646	0.643	0.650
Core decay power	Specified value plus 0.005 MW	Specified value minus 0.008 MW	Specified value plus 0.028 MW	Specified value minus 0.001 MW	Specified value plus 0.001 MW
Gas-liquid inter-phase drag in core	92.9%	96.3%	98.1%	102.6%	89.8%
Film boiling and steam convective heat transfer coefficients in core	85.6%	76.1%	92.6%	92.1%	90.1%
Discharge coefficient through SG relief valve during SG secondary-side depressurization	0.802	0.827	0.806	0.815	0.851
Core exit temperature that initiated SG secondary-side depressurization	623.6 K	623.0 K	622.3 K	623.1 K	623.6 K

TABLE VII
SPEARMAN'S RANK CORRELATION COEFFICIENTS FOR UNCERTAIN PARAMETERS IN THREE DIFFERENT SAMPLE-SIZE CASES

Parameter	59-sample case	93-sample case	124-sample case
Discharge coefficient through break for single-phase liquid and two-phase flow	0.82	0.85	0.79
Core decay power	0.17	0.19	0.13
Gas-liquid inter-phase drag in core	-0.01	0.07	0.03
Film boiling and steam convective heat transfer coefficients in core	-0.48	-0.45	-0.51
Discharge coefficient through SG relief valve during SG secondary-side depressurization	-0.24	-0.29	-0.27
Core exit temperature that initiated SG secondary-side depressurization	0.19	0.15	0.13

VI. SUMMARY

The assessment was conducted in the LSTF integral effect test simulating a PWR 1.9% vessel upper head SBLOCA with an AM measure under an assumption of total-failure of high-pressure injection system of ECCS. The AM measure was the full opening of relief valves in both SGs at the maximum core exit temperature of 623 K. The uncertainty analysis of the LSTF test was performed using the RELAP5/MOD3.3 code to investigate the influences of the uncertain parameters on the PCT. The major outcomes are summarized as follows.

The LSTF test satisfied the requirements for the appropriate integral effect test through the description of the experiment against the foremost criteria. The late and slow response of the core exit thermocouples during core boil-off caused a substantial increase in the cladding surface temperature. The entire core quench occurred because of loop seal clearing in both loops induced by the ACC system actuation.

The RELAP5 code underpredicted the primary pressure due to the overprediction of the break flow rate during two-phase flow discharge period. The upper head collapsed liquid level was not properly calculated during two-phase flow discharge period. The core exit temperature was not well predicted due to a limitation to the estimation of multi-dimensional steam flow in the core. The PCT was underpredicted due to the insufficient estimations of the collapsed liquid levels of the crossover leg downflow-side and the core.

The uncertainty analysis results showed that the sample size with regard to the order statistics affected the PCT value with a 95% probability at a 95% confidence level, and the Spearman's rank correlation coefficient. The combination of the C_d through the break for single-phase liquid and two-phase flow, the film

boiling and steam convective heat transfer coefficients in the core, and the C_d through the SG relief valve during the SG secondary-side depressurization proved to be largely sensitive for the PCT within the defined uncertain ranges.

ACKNOWLEDGMENT

The author would like to thank Messrs. M. Ogawa and A. Ohwada of Japan Atomic Energy Agency for carrying out the LSTF test under collaboration with members from Nuclear Engineering Co. as well as Miss K. Toyoda of Research Organization for Information Science and Technology for manipulating the experimental data.

REFERENCES

- [1] F. Menzel, G. Sabundjian, F. D'Auria, and A. Madeira, "Proposal for systematic application of BEPU in the licensing process of nuclear power plants," *Int. J. Nucl. Energy Sci. Technol.*, vol. 10, 2016, pp. 323–337.
- [2] A. Annunziato, H. Glaeser, J. Lillington, P. Marsili, C. Renault, and A. Sjoberg, "CSNI Integral Test Facility Validation Matrix for the Assessment of Thermal-Hydraulic Codes for LWR LOCA and Transients," NEA/CSNI/R(96)17, 1996.
- [3] N. Aksan, F. D'Auria, H. Glaeser, J. Lillington, R. Pochard, and A. Sjoberg, "Evaluation of the CSNI Separate Effects Tests (SET) Validation Matrix," CSNI report OECD/GD(97)9, 1996.
- [4] T. Skorek, "Input uncertainties in uncertainty analyses of system codes: Quantification of physical model uncertainties on the basis of CET (combined effect test)," *Nucl. Eng. Des.*, vol. 321, 2017, pp. 301–317.
- [5] D. Bestion, F. D'Auria, P. Lien, and H. Nakamura, "A state-of-the-art report on scaling in system thermal-hydraulics applications to nuclear reactor safety," NEA/CSNI/R(2016)14, 2017.
- [6] The ROSA-V Group, "ROSA-V Large Scale Test Facility (LSTF) System Description for the Third and Fourth Simulated Fuel Assemblies," JAERI-Tech 2003-037, Japan Atomic Energy Research Institute, Ibaraki, Japan, 2003.
- [7] K. Umminger, L. Dennhardt, S. Schollenberger, and B. Schoen, "Integral Test Facility PKL: Experimental PWR Accident Investigation," *Sci.*

- Technol. Nucl. Installations, Article ID 891056, vol. 2012, 2012, pp. 1–16.
- [8] K.Y. Choi, Y.S. Kim, C.H. Song, and W.P. Baek, “Major Achievements and Prospect of the ATLAS Integral Effect Tests,” *Sci. Technol. Nucl. Installations*, Article ID 375070, vol. 2012, 2012, pp. 1–18.
- [9] USNRC, “Reactor Pressure Vessel Head Degradation and Reactor Coolant Pressure Boundary Integrity,” *Bulletin 2002-01, OMB Control No.: 3150-0012*, U.S. Nuclear Regulatory Commission, Washington, DC, 2002.
- [10] USNRC, “Davis-Besse Reactor Pressure Vessel Head Degradation: Overview, Lessons Learned, and NRC Actions Based on Lessons Learned,” *NUREG/BR-0353, Rev. 1*, U.S. Nuclear Regulatory Commission, Washington, DC, 2008.
- [11] H. Shiroyama, “Regulatory failures of nuclear safety in Japan—the case of Fukushima accident,” in: *Proc. of the Earth System Governance Tokyo Conference: Complex Architectures, Multiple Agents, Earth System Governance*, Tokyo, Japan, January 2013.
- [12] Y. Kukita, K. Tasaka, H. Asaka, T. Yonomoto, and H. Nakamura, “The effects of break location on PWR small break LOCA: experimental study at the ROSA-IV LSTF,” *Nucl. Eng. Des.*, vol. 122, 1990, pp. 255–262.
- [13] T. Takeda, “ROSA/LSTF test and RELAP5 code analyses on PWR 1% vessel upper head small-break LOCA with accident management measure based on core exit temperature,” *Nucl. Eng. Technol.*, vol. 50, 2018, pp. 1412–1420.
- [14] USNRC Nuclear Safety Analysis Division, “RELAP5/MOD3.3 Code Manual,” *NUREG/CR-5535/Rev 1*, Information Systems Laboratories, Inc., 2001.
- [15] T. Takeda, “ROSA/LSTF test and RELAP5 code analyses on PWR hot leg small-break LOCA with accident management measure based on core exit temperature and PKL counterpart test,” *Ann. Nucl. Energy*, vol. 121, 2018, pp. 594–606.
- [16] T. Takeda, “Uncertainty analysis of ROSA/LSTF test on pressurized water reactor cold leg small-break loss-of-coolant accident without scram,” *Int. J. Nucl. Quantum Eng.*, vol. 13, 2019, pp. 82–90.
- [17] N. Zuber, “Problems in Modeling Small Break LOCA,” *NUREG-0724*, USNRC, Washington, DC, 1980.
- [18] NEA, “Final Integration Report of OECD/NEA ROSA Project 2005–2009,” *NEA/CSNI/R(2013)1*, 2013.
- [19] H. Austregesilo, B. Krzykacz-hausmann, and T. Skorek, “Uncertainty and sensitivity analysis of results of the posttest calculation of a LSTF experiment with the code ATHLET,” *GRS Annual Report 2008*, 2008, pp. 35–41.
- [20] J. Freixa and A. Manera, “Analysis of an RPV upper head SBLOCA at the ROSA facility using TRACE,” *Nucl. Eng. Des.*, vol. 240, 2010, pp. 1779–1788.
- [21] C. Queral, J. Gonzalez-cadelo, G. Jimenez, and E. Villalba, “Accident management actions in an upper-head small-break loss-of-coolant accident with high-pressure safety injection failed,” *Nucl. Technol.*, vol. 175, 2011, pp. 572–593.
- [22] H. Kumamaru and K. Tasaka, “Recalculation of Simulated Post-scrum Core Power Decay Curve for Use in ROSA-IV/LSTF Experiments on PWR Small-break LOCAs and Transients,” *JAERI-M 90-142*, Japan Atomic Energy Research Institute, Ibaraki, Japan, 1990.
- [23] H.K. Fauske, “The discharge of saturated water through tubes,” *AIChE Symp. Ser.*, vol. 61, 1965, pp. 210–216.
- [24] K.H. Ardron and R.A. Furness, “A study of the critical flow models used in reactor blowdown analysis,” *Nucl. Eng. Des.*, vol. 39, 1976, pp. 257–266.
- [25] D.W. Sallet, “Thermal hydraulics of valves for nuclear applications,” *Nucl. Sci. Eng.*, vol. 88, 1984, pp. 220–244.
- [26] T. Takeda, A. Ohnuki, and H. Nishi, “RELAP5 code study of ROSA/LSTF experiments on PWR safety system using steam generator secondary-side depressurization,” *J. Energy Power Eng.*, vol. 9, 2015, pp. 426–442.
- [27] A. Guba, M. Makai, and L. Pál, “Statistical aspects of best estimate method-I,” *Reliability Eng. Syst. Safety*, vol. 80, 2003, pp. 217–232.
- [28] IAEA, “Best Estimate Safety Analysis for Nuclear Power Plants: Uncertainty Evaluation,” *IAEA Safety Reports Series No. 52*, Vienna, Austria, 2008.
- [29] A. de Crécy, P. Bazin, H. Glaeser, H., et al., “Uncertainty and sensitivity analysis of the LOFT L2-5 test: Results of the BEMUSE programme,” *Nucl. Eng. Des.*, vol. 238, 2008, pp. 3561–3578.
- [30] W.W. Daniel, “Spearman rank correlation coefficient,” *Applied Nonparametric Statistics (second ed.)*, PWS-Kent Publishing, Boston, MA, 1990.
- Takeshi Takeda** is on loan to Nuclear Regulation Authority from Japan Atomic Energy Agency. His interests include thermal-hydraulic safety during accidents and abnormal transients of light water reactor through experiments using test facilities and by calculations with best-estimate computer code.